Chinese Chemical Letters 35 (2024) 109150

Contents lists available at ScienceDirect

Chinese Chemical Letters

journal homepage: www.elsevier.com/locate/cclet

Legumain-triggered aggregable gold nanoparticles for enhanced intratumoral retention

Zhi Li[a], Wenpei Li[a], Shaoping Jiang[a], Chuan Hu[b], Yuanyu Huang[a], Maxim Shevtsov[c], Huile Gao[b,*], Shaobo Ruan[a,*]

[a] Advanced Research Institute of Multidisciplinary Sciences, School of Life Science, Beijing Institute of Technology, Beijing 100081, China
[b] Key Laboratory of Drug Targeting and Drug Delivery System, West China School of Pharmacy, Sichuan University, Chengdu 610041, China
[c] Institute of Cytology of Russian Academy of Sciences (RAS), St. Petersburg 194064, Russia

ARTICLE INFO

Article history:
Received 24 July 2023
Revised 22 September 2023
Accepted 24 September 2023
Available online 26 September 2023

Keywords:
Legumain
Size-tunable
Enhanced retention
Stimulus-responsive
Nanomedicine

ABSTRACT

Insufficient intratumoral retention of nanomedicines remains the major challenge for broad implementation in clinical sets. Herein, we proposed a legumain-triggered aggregable gold nanoparticle (GNP) delivery platform (GNPs-A&C). GNPs-A&C could form intratumoral or intracellular aggregates in response to the overexpressed legumain. The aggregates with size increase not only could reduce back-flow from interstitial space to peripheral bloodstream but also could restrict the cellular exocytosis, leading to enhanced intratumoral retention. *In vitro* studies demonstrated that GNPs-A&C possessed an excellent legumain responsiveness and the increased size was closely relevant with legumain expression. *In vivo* studies demonstrated GNPs-A&C possessed slower clearance rate and much higher intratumoral retention within legumain-overexpressed tumor compared to non-aggregable NPs, regardless of intravenous or intratumoral injection. More importantly, this delivery platform significantly improved the chemotherapeutic effect of doxorubicin (DOX) towards subcutaneous xenograft C6 tumor. The effectiveness of this stimulus-responsive aggregable delivery system provides a thinking for designing more intelligent size-tunable nanomedicine that can substantially improve intratumoral retention.

Advances in nanotechnology has endowed nanomedicine with improved disease diagnosis, treatment, and prevention functionalities, especially in cancer management [1,2]. Nanomedicine for cancer therapy is advantageous over conventional medicine owing to their potential to protect from degradation, improve pharmacokinetic profile, enable tumor-targeting delivery *via* either passive targeting or active targeting mechanism, as well as enable simultaneous delivery of multiple therapeutic drugs for combination therapy [3–5]. To date, a large number of nanomedicines or nanoparticle-based drug delivery systems have been developed and documented in both preclinical studies and clinical sets. Despite promising results in preclinical studies, their clinical benefits in cancer patients remain unsatisfied and vary between patients, leading to very low clinical translation rate [6]. Only few nanomedicines are currently approved for clinical application, such as Doxil [7] and Abraxane [8]. One of the major reasons hindering the translation from bench works to clinical application is the insufficient intratumoral retention.

For systemic injected nanomedicine, the delivery of nanomedicine to tumor site and tumor cells is long process. During this process, a series of physiological and pathological barriers may prevent their access to tumor cells, including mononuclear phagocytosis system (MPS) clearance, binding site barriers, elevated interstitial fluid pressure (IFP) and dense extracellular matrix (ECM) [9–12]. Rational design of nanomedicine is thereby highly demanded to circumvent these delivery barriers while achieve improved intratumoral retention. Camouflaging nanomedicine surface with poly(ethylene glycol) (PEG) [13] or naturally-derived cell membrane [14] has been considered as common strategies to reduce MPS clearance and improve blood circulation time. Further modification with ligand to recognize specific receptors on tumor cells is widely used for active targeting delivery and reducing non-specific distribution [15,16]. However, prolonged blood circulation time and improved targeting specificity cannot guarantee sufficient intratumoral retention because of the elevated IFP and dense ECM. For example, several head-to-head comparisons between active and passive targeting demonstrated a lack of significant difference in intratumoral retention [17–19]. Therefore, how to overcome

* Corresponding authors.
E-mail addresses: gaohuile@scu.edu.cn (H. Gao), ruanshaobo@bit.edu.cn (S. Ruan).

https://doi.org/10.1016/j.cclet.2023.109150
1001-8417/

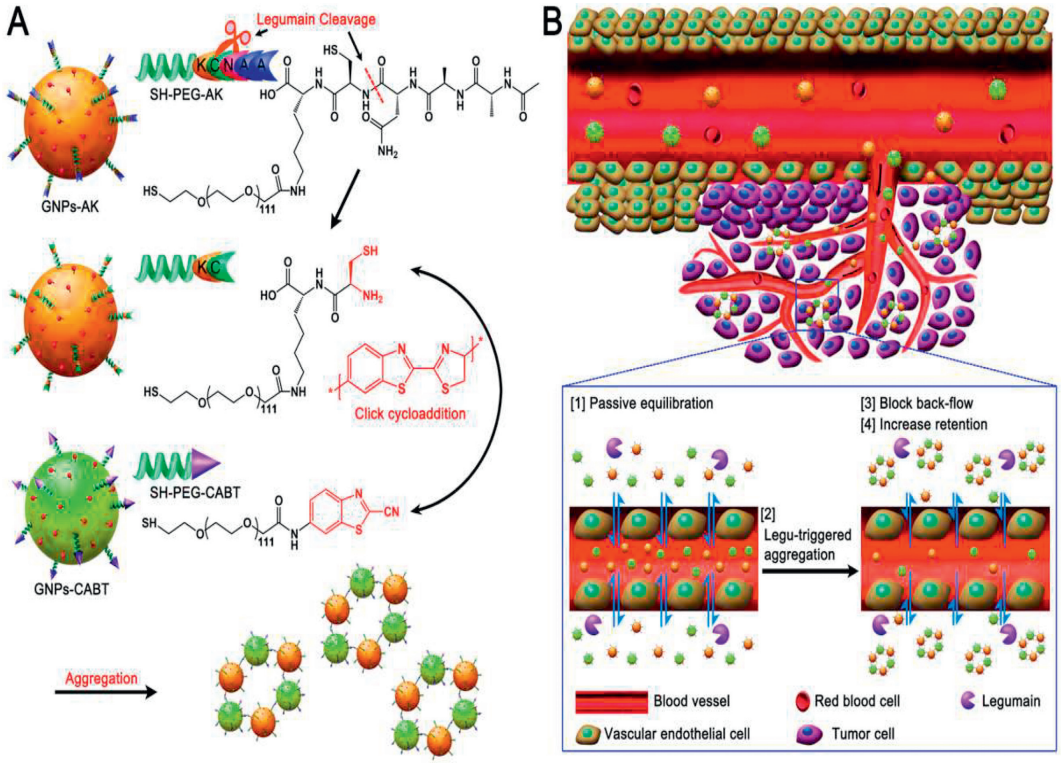

Scheme 1. (A) Schematic diagram of construction and mechanism of legumain-induced aggregation. (B) Schematic diagram of mechanism of GNPs-A&C in enhancing intratumoral retention.

elevated IFP and dense ECM simultaneously to achieve enhanced retention is of great importance.

The physicochemical properties of nanoparticles (NPs), such as size, shape, surface charge, play a critical role in governing intratumoral transport of NPs, especially for those designed for passive targeting *via* enhanced permeability retention (EPR) effect [20–22]. Among these, size is a particularly important factor and different size may exhibit distinct transport performance [23–25]. The general consensus is that smaller NPs are more likely to penetrate through dense ECM into deep tumor site, whereas are also easily re-enter peripheral bloodstream under high IFP, leading to poor retention. By contrast, larger NPs are characterized by relatively poor penetration efficiency, but are more likely to retain at the immediate vicinity of vascular extravasation region [26–28]. The different size requirements for retention and penetration pose a challenge for customizing the NP's size in an ideal range. Conventional NPs with constant size are unable to meet the different requirements simultaneously [24]. Therefore, how to integrate the advantages of both smaller and larger NPs to enhance intratumoral retention and penetration simultaneously is greatly important. Fortunately, size-tunable nanoparticles in response to different endogenous or exogenous stimuli have emerged as a promising strategy by taking advantage of different size [24,29-32]. Particularly, stimulus-responsive aggregable NPs represents the most popular strategy. NPs with a small initial size are able to extravasate through the leaky tumor vasculature and penetrate into deep stromal space, then NPs can undergo aggregation in response to specific stimulus, leading to increased size. The aggregated NPs thus block their back-flow from interstitial space into bloodstream, leading to enhanced intratumoral retention.

In this study, we proposed a legumain-triggered aggregable gold nanoparticle delivery system for enhancing the intratumoral retention of doxorubicin (DOX), a chemotherapeutic drug. This delivery system (GNPs-A&C) was consisted of Ala-Ala-Asn-Cys-Lys (AK peptide)-modified GNPs (GNPs-AK) and 2-cyano-6-aminobenzothiazole (CABT)-modified GNPs (GNPs-CABT) (Scheme 1). *In vitro* study demonstrated significant size increase of GNPs-A&C after incubation in C6 cell supernatant for 48 h. *In vivo* studies demonstrated slower clearance rate and higher intratumoral retention of GNPs-A&C in legumain-sufficient C6 tumor compared to non-aggregable PEGylated GNPs (GNPs-PEG), regardless of intravenous or intratumoral injection. Importantly, GNPs-A&C could significantly enhance the intratumoral concentration of DOX and thus delay tumor growth without causing obvious cytotoxicity. The effectiveness of this strategy provides a thinking for designing more intelligent size-tunable nanomedicines to achieve enhanced intratumoral retention.

Dynamic laser scattering (DLS) analysis showed increased hydrodynamic size and zeta potential of GNPs-AK and GNPs-CABT compared to bare GNPs, indicating that GNPs-AK and GNPs-CABT were successfully constructed (Table S1 in Supporting information). To determine the legumain-responsive aggregation of GNPs-A&C, we first evaluated the legumain expression in different cell lines (C6, 4T1, C26, B16F10 and MDA-MB-231 cells). Western blot (WB) analysis showed that C6 cell possessed a highest legumain expression (Fig. 1A). Given that the secretome secreted by cells contains multiple active tumor-associated proteins, including legumain, the supernatant may be used as legumain source for triggering aggregation of GNPs-A&C [33–35]. We directly detected the secreted legumain level in the different cell supernatant using enzyme-linked immunosorbent assay (ELISA) kit. Similarly, the secreted legumain level in C6 cell supernatant was much higher than that in 4T1, C26, B16F10 and MDA-MB-231 cell supernatant, which was in line with the WB analysis (Fig. 1B). Nest, we evaluated whether GNPs-A&C could actually form aggregates in these supernatants. DLS analysis demonstrated that the hydrodynamic size of GNPs-A&C in C6 cell supernatant increased from 40.9 ± 1.2 nm to 226.2 ± 14.6 nm after 48 h incubation (Fig. 1C). Although the size increase of GNPs-A&C in C6 cell supernatant was lower than that incubated in legumain-containing phosphate buffer saline

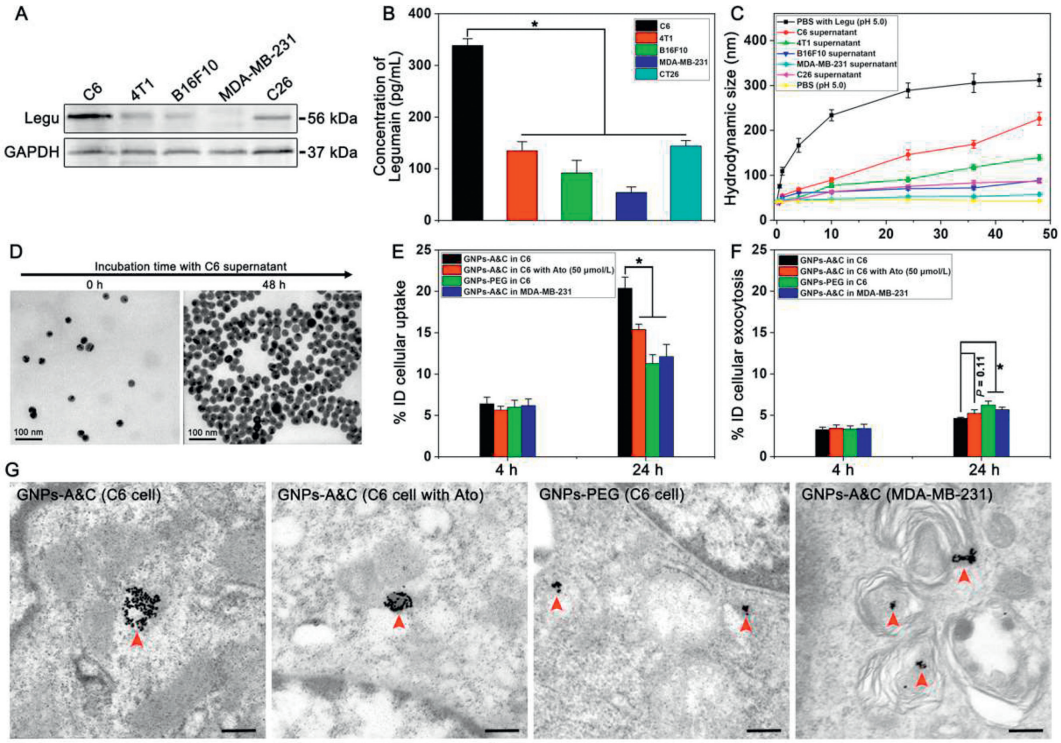

Fig. 1. Evaluation of legumain responsiveness. (A) WB analysis of legumain expressed by different cells. GAPDH was served as a control. (B) ELISA analysis of the concentration of legumain in supernatant from different cells. (C) Hydrodynamic size of GNPs-A&C after resuspended in different cell supernatant at different time intervals, GNPs-A&C incubated in pH 5.0 PBS with or without legumain were served as controls ($n = 3$). (D) TEM images of GNPs-A&C in C6 cell supernatant after 48 h incubation, scale bar: 100 nm. ICP-MS analysis of intracellular gold content in C6 cells (E) and in supernatant (F) after treatment with different formulations ($n = 3$). (G) TEM images of cells treated with different formulations, red arrows indicate GNPs aggregates, scale bar: 200 nm. All data were represented as mean ± standard deviation (SD). $^*P < 0.05$.

(PBS) at 48 h (312.1 ± 13.8 nm), it was much higher than that incubated in 4T1, B16F10, MDA-MB-231 and C26 cell supernatant. Moreover, the size increase was positively correlated with the secretion level of legumain. To exclude the possibility that the size change in different cell supernatant was attributed to the secreted proteins, we determined the size of different cell supernatant at different time intervals. The hydrodynamic size of different cell supernatant was 5–10 nm and showed almost no change even after 48 h incubation (Fig. S1 in Supporting information). These results further proved that the size change of GNPs-A&C was due to the legumain-triggering aggregation instead of large secreted proteins. Meanwhile, size of GNPs-AK, GNPs-CABT and GNPs-PEG showed very slight increase after 48 h incubation in C6 cell supernatant (Fig. S2 in Supporting information). Moreover, transmission electron microscope (TEM) images further showed an obvious aggregation of GNPs-A&C in C6 cell supernatant, indicating that click reaction was taken place successfully between GNPs-A&C (Fig. 1D, Figs. S3–S6 in Supporting information). In contrast, GNPs-A&C in MDA-MB-231 cell supernatant showed much smaller aggregates composed of only several particles, which was similar to GNPs-PEG in C6 supernatant. All these results suggested that cells can secrete active legumain into supernatant and legumain could trigger the aggregation of GNPs-A&C in a legumain-dependent manner.

To validate our hypothesis that aggregation of GNPs-A&C with increased size could restrict the exocytosis of GNPs-A&C by cells, we further quantitatively detected the intracellular and extracellular gold content using inductively coupled plasma mass spectrometry (ICP-MS). At 4 h, the percentage incubated dose (% ID) of cellular uptake C6 cells treated with GNPs-A&C was 6.40% ± 0.81%, which was similar to C6 treated with GNPs-PEG (5.64% ± 0.48%) and MDA-MB-231 cells treated with GNPs-A&C (5.99% ± 0.85%) (Fig. 1E). At 24 h, the % ID of cellular uptake by C6 cells treated with GNPs-A&C reached 20.4% ± 1.36%, which was 1.56-fold higher than C6 cells treated with GNPs-PEG (11.3% ± 1.08%) and 1.78-fold higher than MDA-MB-231 cells treated with GNPs-A&C (12.1% ± 1.49%). To further determine the exocytosis, we detected the GNPs exocytosed in the cell supernatant. At 4 h, the % ID of cellular exocytosis by C6 cells treated with GNPs-A&C, GNPs-PEG and MDA-MB-231 cells treated with GNPs-A&C was 2.35% ± 0.15%, 2.62% ± 0.08% and 3.34% ± 0.17%, respectively (Fig. 1F). At 24 h, the % ID of cellular exocytosis by C6 cells treated with GNPs-A&C was 2.59% ± 0.44%, which was lower than C6 cells treated with GNPs-PEG (3.85% ± 0.59%) and MDA-MB-231 cells treated with GNPs-A&C (3.81% ± 0.59%). All these results indicated that GNPs-A&C acquired enhanced intracellular retention while reduced exocytosis in legumain-sufficient C6 cells compared to that in legumain-deficient cells, especially at 24 h. This is mainly owing to that the intracellular aggregation of GNPs-A&C with increased size reduced their exocytosis, leading to an improved intracellular retention [36]. To prove legumain responsiveness, we pre-treated C6 cells with atorvastatin (Ato), a legumain inhibitor [37,38]. Compared to GNPs-A&C, the % ID of cellular uptake by Ato+GNPs-A&C co-treated C6 cells reduced, while the % ID of cellular exocytosis increased. This result verified that inhibiting legumain activity reduced the intracellular retention but increased exocytosis, indicating legumain was pivotal for inducing intracellular aggregation of GNPs-A&C. Moreover, when conjugating Cy5.5 onto GNPs-A&C *via* pH sensitive linker [39], the prepared GNPs-Cy5.5-A&C also showed a stronger fluorescence signal than GNPs-Cy5.5-PEG after treatment with C6 cells for 4 h as well as GNPs-Cy5.5-A&C-treated MDA-MB-231 cells (Fig. S7 in Supporting information). Increasing incubation time further enhanced the fluorescence signal of GNPs-Cy5.5-A&C (Fig. S8 in Supporting information), suggesting that GNPs-Cy5.5-A&C also could enhance intracellular retention of their payload in a time-dependent manner.

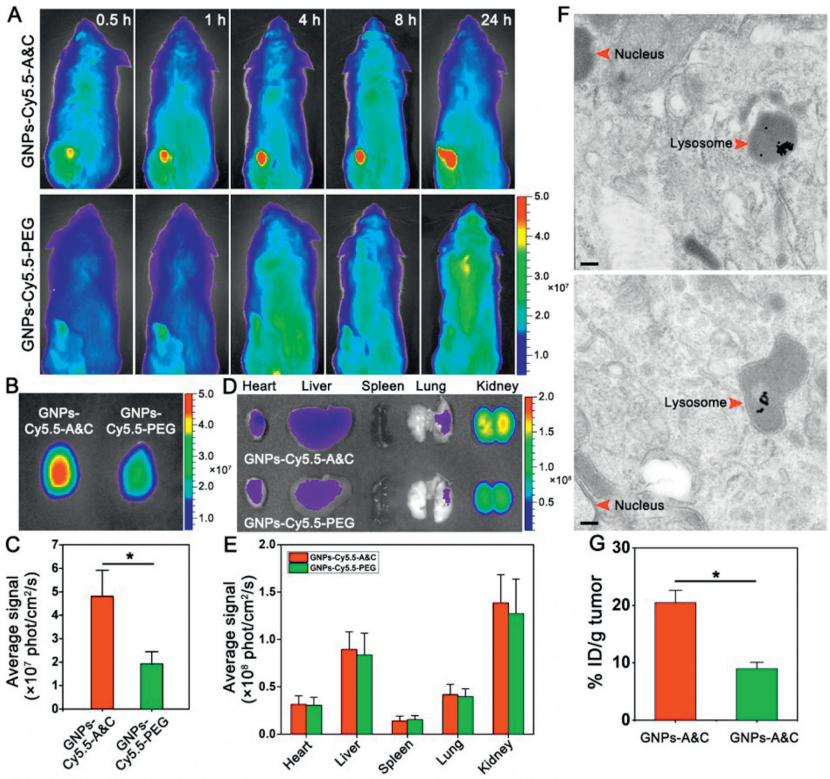

Fig. 2. Evaluation of *in vivo* biodistribution. (A) Living imaging of subcutaneous C6 tumor-bearing mice injected with GNPs-Cy5.5-A&C and GNPs-Cy5.5-PEG. *Ex vivo* imaging of tumors (B) and normal tissues (D) from mice at 24 h post-injection with GNPs-Cy5.5-A&C and GNPs-Cy5.5-PEG. Quantitative analysis of fluorescence intensity from tumors (C) and normal tissues (E) from *ex vivo* imaging. (F) TEM images of C6 tumor slice treated with GNPs-A&C and GNPs-PEG at 24 h post-injection, scale bars: 200 nm. (G) ICP-MS analysis of gold content within tumor at 24 h post-injection with GNPs-A&C and GNPs-PEG ($n = 3$). All data were represented as mean ± SD. $^*P < 0.05$.

Subsequently, TEM imaging was performed to prove the ability of GNPs-A&C to form intracellular aggregates. Images demonstrated obvious GNPs aggregates in C6 cells treated with GNPs-A&C for 24 h, whereas much smaller GNPs aggregates in C6 cells treated with GNPs-PEG as well as in MDA-MB-231 cells post-treatment with GNPs-A&C (Fig. 1G). Compared to GNPs-A&C treated C6 cells, smaller GNPs aggregates were also found in Ato+GNPs-A&C co-treated C6 cells. These images clearly suggested that GNPs-A&C could indeed form intracellular aggregates in the presence of legumain. Also, the size of aggregate was proportion to the legumain expression and activity, which well explained the reduced exocytosis of GNPs-A&C by C6 cells compared to control groups.

GNPs-A&C was further conjugated with pH sensitive DOX prodrug to obtain GNPs-DOX-A&C following our previous study [40]. The cell viability after treatment with GNPs-DOX-A&C, GNPs-DOX-PEG and free DOX decreased gradually over time (Fig. S9A in Supporting information). However, the difference between C6 cells treated with GNPs-DOX-A&C and GNPs-DOX-PEG increased over time, indicating the legumain-triggering aggregation of GNPs-DOX-A&C was beneficial for enhancing cytotoxicity of DOX. This was mainly due to that GNPs-DOX-A&C had a higher intracellular retention than GNPs-DOX-PEG, thus resulting in higher intracellular accumulation of DOX. Moreover, the Annexin FITC-PI double staining assay was performed to further determine apoptosis and necrosis (Figs. S9B and C in Supporting information). 24 h post-incubation, the percentage of apoptosis and necrosis of C6 cells treated with GNPs-DOX-A&C were 47.45% ± 0.04% and 23.90% ± 0.03%, respectively, which was higher than that treated with GNPs-DOX-PEG (43.10% ± 0.05% and 14.40% ± 0.03%). This result further confirmed that aggregable GNPs-DOX-A&C was able to induce higher apoptosis and necrosis compared to non-aggregable GNPs-DOX-PEG.

In vivo biodistribution and tumor-targeting effect were determined by intravenously injecting GNPs-Cy5.5-A&C into subcutaneous C6 tumor-bearing mice. The animal experiments were carried out under the supervision of the Animal Care and Use Committee of Beijing Institute of Technology. Living imaging demonstrated that the fluorescence signal of GNPs-Cy5.5-A&C was precisely located at tumor site and the intensity increased as time went on (Fig. 2A). By contrast, the fluorescence intensity of GNPs-Cy5.5-PEG was much lower than that of GNPs-Cy5.5-A&C, suggesting that GNPs-Cy5.5-A&C not only could specifically deliver to tumor site, but also acquire a higher intratumoral retention. Moreover, *ex vivo* imaging of tumors collected at 24 h post-injection, semi-quantitative analysis as well as immunofluorescence staining further supported this finding (Figs. 2B and C, Fig. S10 in Supporting information). The higher intratumoral retention of GNPs-Cy5.5-A&C may be attributed to the aggregates with increased size blocked the back-flow from tumor stroma to peripheral bloodstream. *Ex vivo* imaging of normal tissues and semi-quantitative analysis displayed that the fluorescence signal of GNPs-Cy5.5-A&C and GNPs-Cy5.5-PEG were mainly distributed at kidney and liver after systemic injection, suggesting that kidney and liver were the major organs involving in clearance of both NPs (Figs. 2D and E).

Next, we assessed whether GNPs-A&C could actually form intratumoral aggregates. TEM image of C6 tumor slice treated with GNPs-A&C demonstrated clear aggregates within lysosome, whereas C6 tumor treated with GNPs-PEG demonstrated much smaller aggregates and even individual NP (Fig. 2F). This result clearly confirmed the *in vivo* aggregable capacity of GNPs-A&C. Moreover, we evaluated whether the formation of aggregates could enhance the intratumor retention of GNPs-A&C. After intravenous injection, ICP-MS analysis showed that the % ID per gram C6 tumor treated with GNPs-A&C was as high as 20.5% ± 2.1%, which

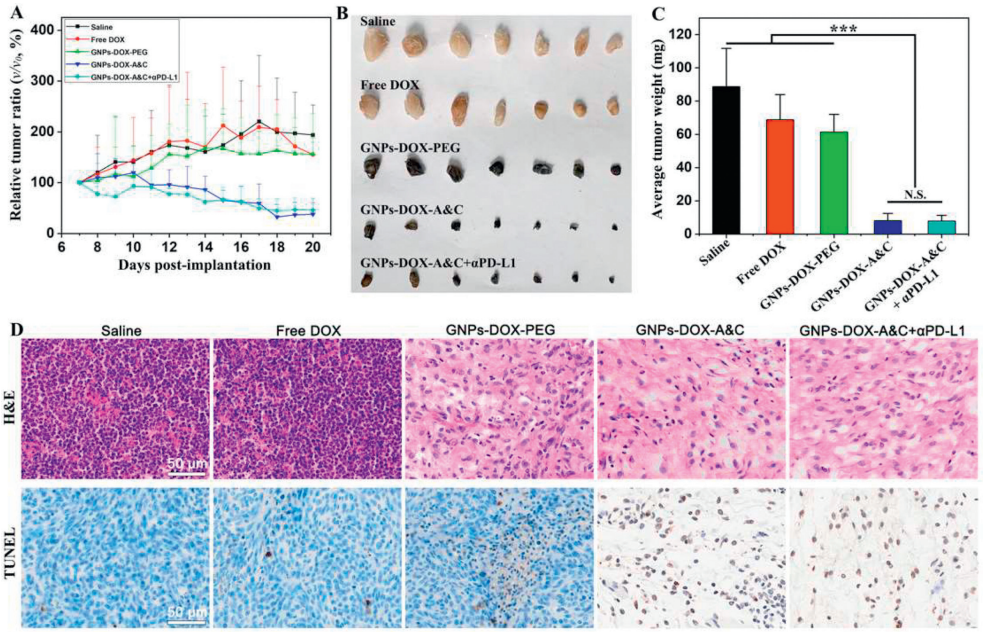

Fig. 3. Evaluation of the anti-tumor effect. (A) Percentage of relative tumor growth rate during and post-treatment with different formulations, V_0 indicated the initial tumor volume. (B) Photograph of tumors collected from mice in each group on Day 20. (C) Average tumor weight of each group on Day 20. (D) H&E and TUNEL staining of tumor slices after treatment with different formulations, scale bars: 50 μm. Data were represented as mean ± SD. $^{***}P < 0.001$. N.S. indicated no significance.

was much higher than that treated with GNPs-PEG (8.9% ± 1.1%) (Fig. 2G). This result strongly supported our hypothesis that the formation of intratumor aggregates could block their back-flow to bloodstream, leading to reduced clearance rate and enhanced retention.

To further prove that GNPs-A&C could reduce clearance rate, we next established a mouse model bearing two C6 subcutaneous tumor on both side of upper thigh. Subsequently, GNPs-Cy5.5-A&C and GNPs-Cy5.5-PEG were intratumorally injected into left C6 tumor and right one, respectively. *In vivo* fluorescence imaging showed similar fluorescence intensity at both tumors at 0.5 h, suggesting the GNPs-Cy5.5-A&C and GNPs-Cy5.5-PEG possessed a similar initial clearance rate (Fig. S11A in Supporting information). With the time extended, the fluorescence signal in the left tumor increased to a highest intensity at 24 h and then decreased to a relatively low intensity at 48 and 72 h. By contrast, the fluorescence signal in the right tumor was much lower, suggesting that GNPs-Cy5.5-A&C possessed lower clearance rate than GNPs-Cy5.5-PEG. Quantitative analysis of fluorescent signal and immunofluorescence staining of tumor slices further supported the notion that GNPs-Cy5.5-PEG possessed a higher intratumoral retention (Figs. S11B and C in Supporting information). These results indicated that the legumain-responsive aggregable GNPs-Cy5.5-A&C was able to reduce clearance from tumor stroma to peripheral bloodstream by increasing their size compared to non-aggregable NPs.

Encouraged by the *in vivo* distribution, we set out to evaluate the anti-tumor effect of GNPs-DOX-A&C against subcutaneous C6 xenograft, as well as the anti-tumor effect of GNPs-DOX-A&C combined with anti-programmed cell death-ligand 1 (αPD-L1) (Fig. S12 in Supporting information). Compared to saline group, mice treated with free DOX demonstrated similar tumor growth rate, suggesting that free DOX was unable to deliver to tumor site at a sufficient amount (Fig. 3A, Fig. S13 in Supporting information). Mice treated with GNPs-DOX-PEG showed slightly slower tumor growth rate. By contrast, the tumor growth rate in GNPs-DOX-A&C group was much slower than free DOX and GNPs-DOX-PEG group, and showed even negative growth rate. Similar result was also found in mice treated with GNPs-DOX-A&C+αPD-L1. At Day 20, mice were sacrificed and tumors were collected for weighting and photographing. The tumors from GNPs-DOX-A&C or GNPs-DOX-A&C+αPD-L1 group were much smaller than other groups (Fig. 3B), which was supported by tumor weight (Fig. 3C). Together, these results further confirmed that GNPs-DOX-A&C could deliver DOX to tumor site at an enhanced concentration and thus efficiently inhibit tumor growth.

Furthermore, hematoxylin and eosin (H&E) and terminal deoxynucleotidyl transferase-mediated dUTP nick-end labeling (TUNEL) staining of tumor slice were performed to evaluate the necrosis and apoptosis post-treatment. In saline and free DOX groups, H&E staining demonstrated plenty and compact nuclei of C6 tumor cells, and TUNEL staining demonstrated very limited apoptotic bodies, confirming that free DOX was unable to effectively inhibit tumor growth (Fig. 3D). In GNPs-DOX-PEG group, obvious reduction of nuclei and increased number of apoptotic bodies was observed compared to free DOX group. By contrast, the nuclei density in GNPs-DOX-A&C and GNPs-DOX-A&C+αPD-L1 groups was much lower than other groups, and the number of apoptotic bodies was also much higher than other groups. These results indicated that GNPs-DOX-A&C could induce much more necrosis and apoptosis, which was mainly owing to the aggregable GNPs-DOX-A&C could significantly increase the intratumoral concentration of DOX compared to non-aggregable GNPs-DOX-PEG and free DOX.

Moreover, there was no remarkable change of body weight in these groups post-treatment except for free DOX group (Fig. S14 in Supporting information). The body weight in free DOX group demonstrated obvious reduction, implying the severe cytotoxicity of free DOX and these NPs could reduce the cytotoxicity of DOX by reducing non-specific accumulation at normal tissues. Meanwhile, H&E staining of heart displayed typical myocardial injury in free DOX group, confirming that free DOX could induce severe cardiotoxicity (Fig. S15 in Supporting information). By comparison, there were no obvious myocardial injuries in other groups, which was mainly owing to the reduced accumulation of DOX in heart and pH-responsive DOX prodrug was released slowly under normal pH conditions (Fig. S16 in Supporting information). In addition, no obvious pathological abnormalities were observed in

other tissue slices, denoting that GNPs-DOX-A&C possessed good biocompatibility.

To directly assess whether combination therapy led to an improved anti-tumor immune response, we first evaluated the dendritic cells (DCs) activation. Treatment with GNPs-DOX-A&C+αPD-L1 induced a higher population of mature DCs ($CD11c^+CD80^+$ and $CD11c^+CD86^+$) than other treatments, while was similar to GNPs-DOX-A&C treatment (Figs. S17A–D in Supporting information). This result suggested that GNPs-DOX-A&C could induce apoptosis of tumor cells to release tumor-associated antigens (TAAs), which could stimulate DC maturation. Despite that immune checkpoint blockade may promote the DCs maturation has been reported [41], GNPs-DOX-A&C+αPD-L1 showed no significant difference in promoting DC maturation, which may be owing to the subcutaneous C6 tumor are immunogenic. Next, the infiltration and differentiation of T lymphocytes in tumor microenvironment was also determined. On the one hand, a much higher population of both $CD8^+$ T cells and $CD4^+$ T cells infiltrating into the tumor stroma post-treatment with GNPs-DOX-A&C+αPD-L1 compared to other treatment (Fig. S17E in Supporting information). On the other hand, a relatively lower population of $Foxp3^+$ regulatory T (Treg) cells within tumor stroma after treatment with GNPs-DOX-A&C+αPD-L1 compared to other treatments. Together, the combination of αPD-L1 with GNPs-DOX-A&C not only could boost anti-tumor immune response, but also could alleviate immunosuppressive microenvironment, resulting in much improved therapeutic effect.

Although a variety of therapeutic agents are available for cancer treatment, insufficient delivery to target site greatly limits their therapeutic potential used alone or in combination [6]. By using this stimulus-responsive aggregable delivery system, researcher may pursue combination of novel therapeutic agents as long as therapeutic agents can be conjugated onto GNPs. To enable more customized combination strategies, the inner GNPs can be replaced with other NPs to either covalently or non-covalently load therapeutic agents. Moreover, it should be noted that this legumain-responsive aggregation strategy was evaluated in a subcutaneous C6 tumor model. The ability to cross the blood-brain barrier (BBB) should be considered if the intended treatment is toward orthotopic glioma. Encouragingly, various BBB-crossing delivery strategies [42–44] have been developed for combining this aggregation strategy to enhance accumulation and selectivity within glioma simultaneously.

In conclusion, we constructed a legumain-responsive aggregable NPs delivery system, GNPs-A&C, for enhancing the intratumoral retention. GNPs-A&C could form aggregates *via* legumain-triggered click reaction, resulting in size increase. *In vitro* and *in vivo* studies demonstrated GNPs-A&C could indeed form aggregates and enhance intratumoral retention compared to GNPs-PEG. More importantly, GNPs-DOX-A&C could significantly improve the chemotherapeutic effect by substantially increasing the intratumoral accumulation of DOX. Combination of GNPs-DOX-A&C with immune checkpoint inhibitor further enhanced the inhibitory effect by boosting anti-tumor immune response. The effectiveness of this strategy provided thinking for engineering stimulus-responsive size-tunable nanoplatform for improving intratumoral accumulation of therapeutic agents.

Declaration of competing interest

The authors declare that they have no known competing financial interests or personal relationships that could have appeared to influence the work reported in this paper.

Acknowledgments

This work was supported by the Beijing Natural Science Foundation (No. L222128), Beijing Institute of Technology Research Fund Program for Young Scholars (No. XSQD-202121010) and National Natural Science Foundation of China (No. 81961138009).

Supplementary materials

Supplementary material associated with this article can be found, in the online version, at doi:10.1016/j.cclet.2023.109150.

References

[1] H. Chen, W. Zhang, G. Zhu, et al., Nat. Rev. Mater. 2 (2017) 17024.
[2] R. Liu, C. Luo, Z.Q. Pang, et al., Chin. Chem. Lett. 34 (2023) 107518.
[3] R.K. Jain, T. Stylianopoulos, Nat. Rev. Clin. Oncol. 7 (2010) 653–664.
[4] A.Z. Wang, R. Langer, O.C. Farokhzad, Annu. Rev. Med. 63 (2012) 185–198.
[5] Y. Dang, J. Guan, Smart Mater. Med. 1 (2020) 10–19.
[6] S. Wilhelm, A.J. Tavares, Q. Dai, et al., Nat. Rev. Mater. 1 (2016) 16014.
[7] Y. Barenholz, J. Control. Release 160 (2012) 117–134.
[8] E. Miele, G.P. Spinelli, E. Miele, et al., Int. J. Nanomed. 4 (2009) 99–105.
[9] E. Blanco, H. Shen, M. Ferrari, Nat. Biotechnol. 33 (2015) 941–951.
[10] Q. Sun, Z. Zhou, N. Qiu, et al., Adv. Mater. 29 (2017) 1606628.
[11] S. Ruan, Y. Zhou, X. Jiang, et al., Adv. Sci. 8 (2021) 2004025.
[12] Y. Liu, Z. Zhao, M. Li, Asian J. Pharm. Sci. 17 (2022) 523–543.
[13] J.S. Suk, Q. Xu, N. Kim, et al., Adv. Drug Deliv. Rev. 99 (2016) 28–51.
[14] B.T. Luk, L. Zhang, J. Control. Release 220 (2015) 600–607.
[15] J.D. Byrne, T. Betancourt, L. Brannon-Peppas, Adv. Drug Deliv. Rev. 60 (2008) 1615–1626.
[16] J. Yoo, C. Park, G. Yi, et al., Cancers 11 (2019) 640.
[17] E.A. Sykes, J. Chen, G. Zheng, et al., ACS Nano 8 (2014) 5696–5706.
[18] X. Huang, X. Peng, Y. Wang, et al., ACS Nano 4 (2010) 5887–5896.
[19] S. Kunjachan, R. Pola, F. Gremse, et al., Nano Lett. 14 (2014) 972–981.
[20] A. Albanese, P.S. Tang, W.C. Chan, Annu. Rev. Biomed. Eng. 14 (2012) 1–16.
[21] M. Zhu, G. Nie, H. Meng, et al., Acc. Chem. Res. 46 (2013) 622–631.
[22] W. Poon, B.R. Kingston, B. Ouyang, et al., Nat. Nanotechnol. 15 (2020) 819–829.
[23] N. Hoshyar, S. Gray, H. Han, et al., Nanomedicine 11 (2016) 673–692.
[24] W. Yu, R. Liu, Y. Zhou, et al., ACS Cent. Sci. 6 (2020) 100–116.
[25] J. Hu, X.W. Yuan, F. Wang, et al., Chin. Chem. Lett. 32 (2021) 1341–1347.
[26] S.D. Perrault, C. Walkey, T. Jennings, et al., Nano Lett. 9 (2009) 1909–1915.
[27] X. Liu, Y. Chen, H. Li, et al., ACS Nano 7 (2013) 6244–6257.
[28] A. Albanese, A.K. Lam, E.A. Sykes, et al., Nat. Commun. 4 (2013) 2718.
[29] W. Yu, M. Shevtsov, X.C. Chen, et al., Chin. Chem. Lett. 31 (2020) 1366–1374.
[30] X.D. Xue, H.J. Qu, Y.P. Li, Exploration 2 (2022) 2021013.
[31] Y.L. Song, H.Q. Jing, L.B. Vong, et al., Chin. Chem. Lett. 33 (2022) 1705–1717.
[32] J.Y. Sun, J.Y. Li, X. Li, et al., Chin. Chem. Lett. 34 (2023) 107891.
[33] S.T. Chen, T.L. Pan, H.F. Juan, et al., J. Proteome Res. 7 (2008) 1379–1387.
[34] C.A. Formolo, R. Williams, H. Gordish-Dressman, et al., J. Proteome Res. 10 (2011) 3149–3159.
[35] X. Gong, A.K. Sharma, M.S. Strano, et al., ACS Nano 8 (2014) 9126–9136.
[36] B.D. Chithrani, W.C. Chan, Nano Lett. 7 (2007) 1542–1550.
[37] R. Solberg, R. Smith, M. Almlof, et al., Biol. Chem. 396 (2015) 71–80.
[38] S. Ruan, C. Hu, X. Tang, et al., ACS Nano 10 (2016) 10086–10098.
[39] S. Ruan, Q. He, H. Gao, Nanoscale 7 (2015) 9487–9496.
[40] S. Ruan, M. Yuan, L. Zhang, et al., Biomaterials 37 (2015) 425–435.
[41] Y. Ge, H. Xi, S. Ju, et al., Cancer Lett. 336 (2013) 253–259.
[42] Q. Guo, Q. Zhu, T. Miao, et al., J. Control. Release 303 (2019) 117–129.
[43] J. Ni, T. Miao, M. Su, et al., J. Control. Release 329 (2021) 934–947.
[44] N.U. Khan, J. Ni, X. Ju, et al., Acta Pharm. Sin. B 11 (2021) 1341–1354.